JOURNAL OF THERMOPHYSICS AND HEAT TRANSFER
Vol. 23, No. 2, April–June 2009

Effects of Mass of Charge on Loop Heat Pipe Operational Characteristics

Abhijit A. Adoni,* Amrit Ambirajan,† V. S. Jasvanth,† and Dinesh Kumar†
ISRO Satellite Center, Bangalore 560 017, India
and
Pradip Dutta‡
Indian Institute of Science, Bangalore 560012, India

DOI: 10.2514/1.41618

Experimental results on a loop heat pipe, using R134a as the working fluid, indicates that the liquid inventory in the compensation chamber can significantly influence the operating characteristics. The large liquid inventory in the compensation chamber, under terrestrial conditions, can result in loss of thermal coupling between the compensation chamber and the evaporator core. This causes the operating temperature to increase monotonically. This phenomenon, which has been experimentally observed, is reported in this paper. A theoretical model to predict the steady-state performance of a loop heat pipe with a weak thermal link between the compensation chamber and the core, as observed in the experiment, is also presented. The predicted and the experimentally determined temperatures correlate well.

Nomenclature

A	=	area (generally flow area), m^2
A_t	=	area of tooth-wick interface, m^2
D	=	diameter, m
F_{LHP}	=	energy imbalance in the evaporator core and compensation chamber, W
H	=	heat transfer coefficient, $W \cdot m^{-2} \cdot K^{-1}$
h	=	enthalpy, $J \cdot kg^{-1}$
K	=	wick permeability, m^2
k	=	thermal conductivity, $W \cdot m^{-1} \cdot K^{-1}$
L	=	length, m
L_{cond}	=	length of condenser, m
$L_{\mathrm{condensation}}$	=	length of condensation, m
M	=	mass, mass of working fluid, kg
$\dot{m}$	=	mass flow rate, $kg \cdot s^{-1}$
P	=	pressure, Pa
Q	=	heating rate, W
T	=	temperature, K
t	=	thickness, m
T_{sat}	=	saturation temperature corresponding to a given pressure
U	=	overall heat transfer coefficient, $W \cdot m^{-2} \cdot K^{-1}$
V	=	volume, m^3
x	=	dryness fraction of vapor
β	=	fraction of volume of liquid in the reservoir
ϵ	=	porosity
$\varepsilon_{\mathrm{glob}}$	=	specified heat balance residual %
ϑ	=	normalized energy imbalance
λ	=	conductance, $W \cdot K^{-1}$

Subscripts

b	=	bayonet
c	=	core
cond	=	condenser
e	=	effective
evap	=	evaporator
fg	=	difference in thermodynamic property in liquid and vapor phase
g	=	groove
i	=	inner part of tube
ins	=	insulation
L	=	leak
l	=	liquid
ll	=	liquid line
load	=	refers to heat load applied externally
loop	=	part of the system excluding the reservoir
o	=	outer part of tube
P	=	pressure
r	=	reservoir or compensation chamber/radial
sc	=	subcooler
sink	=	sink of condenser
t	=	tube/evaporator teeth
v	=	vapor/volume in case of specific heat
vl	=	vapor line
w	=	wick
wp	=	wick pore
∞	=	ambient
0	=	just above the meniscus
1	=	exit of the evaporator
2	=	exit of vapor line/entry of condenser.
2cond	=	saturated liquid, point at which condensation is finished in condenser
2scv	=	saturated vapor, end of sensible cooling of vapor in condenser
3	=	exit of condenser/entry to liquid line
4	=	exit of the liquid line and entry to bayonet
4e	=	fluid in the bayonet at the border of compensation chamber and core
5	=	evaporator core

Received 15 October 2008; revision received 22 December 2008; accepted for publication 27 December 2008. Copyright © 2009 by the American Institute of Aeronautics and Astronautics, Inc. All rights reserved. Copies of this paper may be made for personal or internal use, on condition that the copier pay the $10.00 per-copy fee to the Copyright Clearance Center, Inc., 222 Rosewood Drive, Danvers, MA 01923; include the code 0887-8722/09 $10.00 in correspondence with the CCC.

*Engineer, Thermal Systems Group; abhijit@isac.gov.in.
†Engineer, Thermal Systems Group.
‡Professor, Department of Mechanical Engineering.

I. Introduction

A LOOP heat pipe (LHP) is a two-phase heat transport device that has a working principle similar to that of heat pipes, that is, a closed evaporation and condensation cycle being maintained by capillary pumping. The surface tension force induced by a fine pore wick, located in the evaporator, drives the working fluid in the loop.

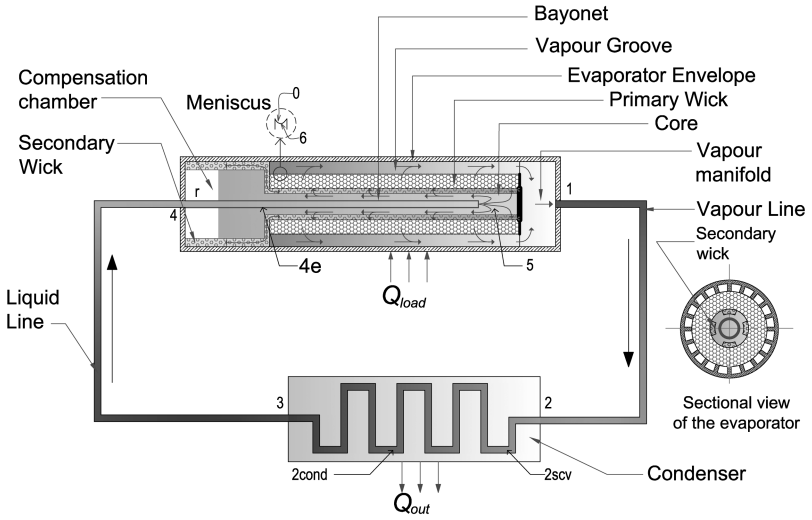

Fig. 1 Schematic of an LHP with a tubular axially grooved evaporator.

The principal feature that distinguishes LHPs from heat pipes is that they do not have a distributed wicking structure. Figure 1 shows a schematic of an LHP. The smooth-walled vapor and liquid lines (tube) connect the capillary evaporator to the condenser. The fine pore-size wick, yielding high capillary pressure, is located only in the evaporator. A two-phase reservoir, often called a compensation chamber (CC), is located alongside the evaporator. The CC allows some controllability of loop temperatures and also accommodates the displaced liquid from the condenser at higher heat loads. The operating principle of LHPs, and the closely related capillary pumped loops (CPLs), is explained in [1–6]. The CPL is a variant of an LHP, with the reservoir plumbed either on the liquid line or directly to the core. A secondary wick is often used in an LHP to ensure that the primary wick is always saturated with liquid and also to provide a good thermal link between the CC and the core. A bayonet is often provided in the evaporator [2,4,7]. In general capillary evaporators can be either *flat plate* (FP) or *tubular axially grooved* (TAG). The principal difference between these evaporators is the shape of the wick; the vapor grooves can either be on the casing or on the wick.

The typical operating temperature (T_0) curve of an LHP is "$\surd$" shaped, when the CC temperature is not externally controlled. At lower heat loads, the LHP is in variable conductance mode, because the CC is not hard-filled and the condensation length depends on the heat load. The constant conductance mode (linear regime) in LHPs with two-phase CC at higher heat loads is due to the opening of the condenser. Linear behavior in LHPs can also be observed when the CC is full of liquid (hard-filled) thereby not allowing the condensation length in the condenser to increase [5].

Ku [1,4] and Maidanik [2] gave a brief chronology of developments in CPLs and LHPs, reviewed advances in CPL/LHP technology, and provided numerous applications. One of the earliest mathematical models of steady-state LHP operation is credited to Dickey and Peterson [8], where the results of a steady-state model of an LHP and comparisons with experimental data are discussed. Kaya and Hoang [9] present a mathematical model for steady-state thermohydraulic performance of an LHP with a two-phase reservoir. The solution procedure assumes that the core and the CC have good thermal coupling, and the thermodynamic state of the core is nearly identical to that of CC. Similarly, Adoni et al. [5] assume that the thermodynamic state of the CC and the core are identical, although no assumption is made about the state of the core, thus making it possible for the model to handle extreme conditions such as hard fill. Guiping et al. [10] experimentally studied operating characteristics of an LHP with dual CC. In this study they compare the LHP performance for various CC orientations. Their design criterion results in hard filling of LHP at higher heat loads (hard filling and condenser opening occur simultaneously). Launay et al. [11] present an analytical approach to the modeling of LHP operating in conventional mode. The results from this model are compared with experimental observation for various working fluids. Hoang et al. [12] highlight the issues related to the terrestrial testing of LHPs in the 1-*g* environment. They attribute significant deviation in operating characteristics of the LHP for different evaporator–CC orientations to the inability of the secondary wick to wet the primary in adverse tilt (i.e., CC relative to the evaporator).

In this paper, the authors present experimental results of an LHP with a TAG evaporator and R134a as the working fluid under

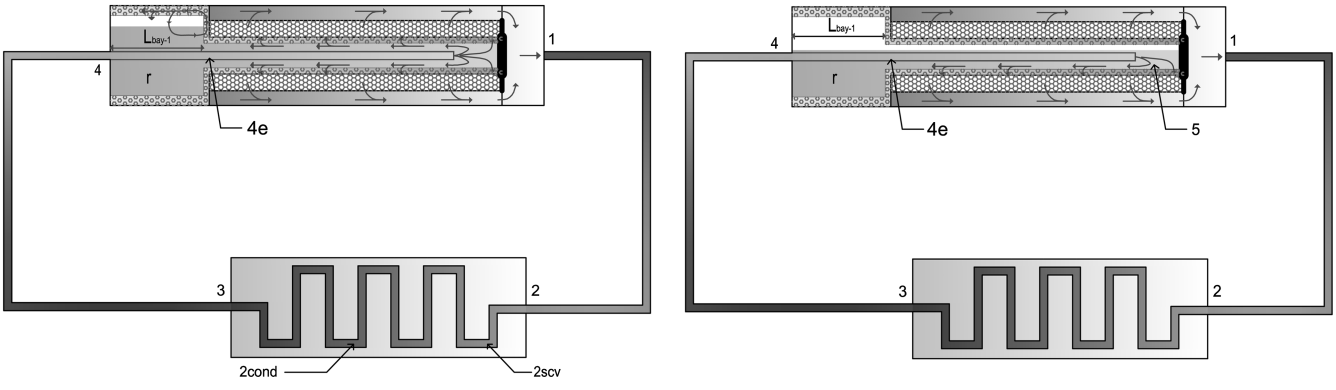

Fig. 2 Schematic showing a) an LHP with bayonet and two-phase CC (large liquid inventory) and no vapor in the core, under terrestrial conditions, and b) an LHP with bayonet and two-phase CC (small liquid inventory) with vapor in the core, under terrestrial conditions.

terrestrial conditions (1-g) and explain the influence of liquid inventory in the CC on an LHP operation. This paper also presents a mathematical model to simulate steady-state operation of an LHP, with a weak thermal link between the CC and the core. This is correlated with the experimental data.

II. Mathematical Model

The mathematical model presented in this section determines the operating temperature and pressure in the loop. This section outlines the methodology to estimate the temperature and pressure at the inlet and the exit of various components of an LHP are indicated in Fig. 1 by 0, 1, 2, 2scv, 2cond, 4, 4e, 5, 6, and r. The nomenclature followed in this paper uses these state points in the subscript of any variable, to represent the physical quantity at that location in the loop, for example, x_4 is the vapor quality at state-point 4. Thermophysical properties of the working fluid are obtained using NIST–REFPROP:7.0 FORTRAN source codes (produced by National Institute of Standards and Technology). These FORTRAN source codes were integrated into the simulation program.

Under terrestrial conditions, if the liquid inventory is large and if the system has a bayonet, the core and the CC will have weak thermal coupling (Fig. 2a). Here, the liquid completely fills the evaporator core, but the CC is partially filled (saturated). The cause of the weak thermal coupling is discussed in greater detail later in Sec. IV. The subcooling associated with the liquid entering the core would be primarily used in maintaining the liquid temperature of the core. Further, under steady-state condition, all the liquid entering the core would move into the wick to compensate for the evaporated liquid. As a result, the fluid in the core can essentially be represented by a subcooled liquid. The CC exchanges heat with the evaporator, the ambient, the core (by conduction), and the bayonet passing through the CC. The heat balance in the CC determines its temperature and pressure. In essence, this LHP behaves like a CPL, where the heat balance in the reservoir determines its temperature and pressure. This LHP cannot tolerate the bubbles entering the core ($x_4 > 0$) unless the secondary wick is present.

The pressure in the core is determined by equating the equation of state for the core with the exit pressure of the liquid line

$$P_5(T_5, \rho_5) = P_4 \tag{1}$$

Note the equation of state $[P_5(T_5, \rho_5)]$ is obtained from REFPROP:7.0. The heat balance in the *core* is given by

$$Q_{Lc}(T_5) = \dot{m} C_{p,54e}(T_5 - T_{4e}) + \lambda_{c-r}(T_5 - T_r) \tag{2}$$

where $C_{p,54e}$ is the mean specific heat of the working fluid between 5 and 4e. The thermodynamic state of the core is determined by simultaneously solving Eqs. (1) and (2). Under steady-state conditions the pressure in the core and the reservoir are equal, the fluid in the CC is saturated and its temperature is determined by

$$T_5 = T_{\text{sat}}(P_5) \tag{3}$$

The energy balance in the *compensation chamber* is given by

$$Q_{r-\infty} = Q_{b-r} + Q_{c-r} + Q_{\text{evap}-r} \tag{4}$$

where Q_{b-r} is the heat exchange between the fluid in the bayonet and the fluid in the CC $[Q_{b-r} = \dot{m} C_{p,4}(T_4 - T_{4e})]$. Q_{b-r} is expanded after substitution for T_{4e} to yield [13]

$$Q_{b-r} = \dot{m} C_{p,4}\left[1 - \exp\left(\frac{-U_{b-r}A_{b-r}}{\dot{m} C_{p,4}}\right)\right](T_4 - T_r) \tag{5}$$

The heat from the core to the CC is given by [13]

$$Q_{c-r} = \lambda_{c-r}(T_5 - T_r) \tag{6}$$

A_{b-r} is the surface area of the bayonet in contact with fluid in the CC. U_{b-r} is the overall heat transfer coefficient between the fluid in the bayonet and that in the reservoir, which is given by

$$\frac{1}{U_{b-r}} = \frac{D_{b,o}}{D_{b,i}H_{b,i}} + \frac{D_{b,i}}{2k_b}\ell_n\left(\frac{D_{b,o}}{D_{b,i}}\right) + \frac{1}{H_{b,o}} \tag{7}$$

The thermodynamic state of the CC is determined by solving Eqs. (3) and (4).

Algorithm A2-LHP, outlined in Fig. 3, is used for calculation of loop temperatures in an LHP with a *subcooled* core and saturated CC. This condition is illustrated in Fig. 2a and discussed earlier in this section. This algorithm is intended for LHPs with weak thermal link between the CC and the core, though the fluidic link between the CC and the core is good. Apart from guessed values of T_0, T_5, and T_r, inputs to this algorithm are Q_{load} and T_{sink}. It is not applicable for the hard-filled reservoir/compensation chamber. This method actually treats the LHP as a CPL with a two-phase reservoir, in which the reservoir temperature is *not* specified externally, rather, it is determined by a heat balance [Eq. (4)]. The algorithm A1-CPL, that is used by A2-LHP is described in [5,13].

The temperatures and pressures in the loop are determined from algorithm A1-CPL [5]. This algorithm evaluates temperatures T_0 to T_6, pressures P_2 to P_4, dryness fractions x_1 to x_4, and mass of

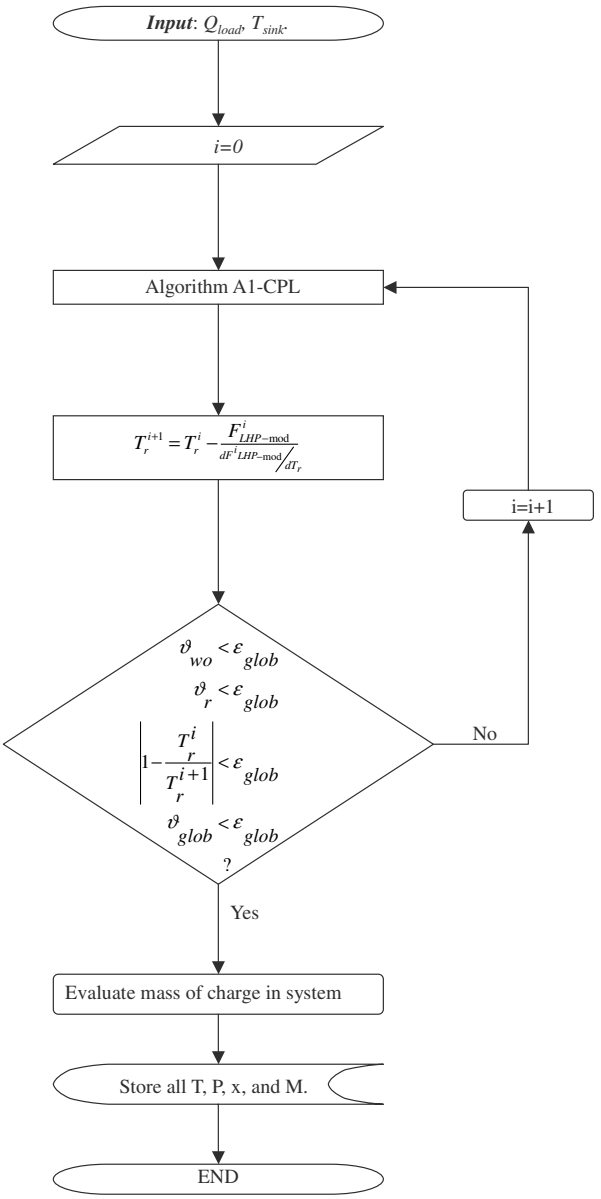

Fig. 3 Algorithm A2-LHP for determination of distribution of temperature, pressure, and mass of working fluid in an LHP with a two-phase compensation chamber with a weak thermal link between the CC and the core, given Q_{load} and T_{sink}.

working fluids in various components. The input parameters to this algorithm are Q_{load}, T_{sink}, and T_r. Equations (1) and (2) are simultaneously solved to determine T_5 and ρ_5 in algorithm A1-CPL. The energy equation in the CC [Eq. (4)] is solved to evaluate T_r using the Newton–Raphson method (NRM) [14]. The energy balance in the CC $F_{\text{LHP-mod}}$ used in A2-LHP for the T_r update equation is defined by

$$F_{\text{LHP-mod}}(T_r) := Q_{b-r} + Q_{c-r} + Q_{\text{evap}-r} - Q_{r-\infty}$$

The derivative $\mathrm{d}F_{\text{LHP-mod}}/\mathrm{d}T_r$ is obtained numerically. The superscript i of $F_{\text{LHP-mod}}$ (as shown in Fig. 3) is the iteration number. In addition to temperature (convergence), convergence is checked for the following heat balance residuals:

$$\vartheta_{wo} := \left| 1 - \frac{\dot{m} h_{fg,1} + Q_{Lo} + Q_{\text{evap}-sh}}{Q_{\text{evap}}} \right| \tag{8}$$

$$\vartheta_r := \left| \frac{F_{\text{LHP-mod}}}{Q_{Lc}} \right| \tag{9}$$

$$\vartheta_{\text{glob}} := \left| 1 - \frac{Q_{\text{vl}} + Q_{\text{ll}} + Q_{\text{cond}} + Q_{\text{evap}-\infty} + Q_{r-\infty}}{Q_{\text{load}}} \right| \tag{10}$$

to ensure that they are less than specified values ($\varepsilon_{\text{glob}}$). The mass of working fluid and the volume fraction of liquid in CC are obtained in the same way as explained in [5]. The numerical scheme [5] used for predicting temperature, pressure, and mass distribution in the loop is a variant of the fixed point iteration technique for a system of nonlinear equations [14]. The NRM is also used to minimize energy balance residual and pressure imbalance.

III. Experimental Setup

Figure 4 shows a schematic of the TAG-evaporator-based LHP along with dimensional details of the experimental setup. The construction and instrumentation details of the TAG evaporator are shown in Fig. 5. The evaporator consists of an envelope enclosing a tubular wick, a vapor manifold, and a liquid inlet plug. The Al6061-T6 envelope is a tube with internal axial vapor grooves. The ultrahigh molecular weight polyethylene (UHMWPE) wick is located in the central hole. Table 1 gives all salient dimensions of the LHP. The condenser is a tube-in-tube heat exchanger and the shell-side fluid forms the sink. The sink temperature (shell-side fluid temperature) is maintained by routing the fluid through a cryostat (constant temperature fluid circulator).

The liquid inlet plug is connected to the CC through a reservoir tube, which is welded to both the CC and the liquid inlet plug. The bayonet, which passes through the CC and the reservoir tube, is connected to the liquid line at the CC wall. The reservoir tube provides a hydraulic link between the CC and the core. This LHP does not have a secondary wick. One of the functions of the secondary wick is to keep the primary wick wetted. Under terrestrial conditions, this is ensured by gravity. The other important function of the secondary wick is to ensure that the CC and core have a good

Table 1 Salient features of a TAG evaporator envelope

Vapor and liquid lines		Condenser	
L_{vl}	1760 mm	L_{cond}	1250 mm
L_{ll}	2310 mm	$D_{\text{cond},o}$	6.35 mm
$D_{\text{vl},o}$, $D_{\text{ll},o}$	6.35 mm	$D_{\text{cond},i}$	4.57 mm
$D_{\text{vl},i}$, $D_{\text{ll},i}$	4.57 mm	$k_{\text{cond},t}$	15 $\text{Wm}^{-1}\text{K}^{-1}$
$k_{\text{vl},t}$, $k_{\text{ll},t}$	15 $\text{Wm}^{-1}\text{K}^{-1}$		
$D_{\text{ins-vl},i}$, $D_{\text{ins-ll},i}$	150 mm		
$H_{\text{vl}-\infty}$	6 $\text{Wm}^{-2}\text{K}^{-1}$		
$H_{\text{ll}-\infty}$	9 $\text{Wm}^{-2}\text{K}^{-1}$		
Evaporator envelope		Reservoir tube	
L_{evap}	200 mm	L_{rt}	60 mm
$D_{\text{evap},o}$	45 mm	$D_{rt,i}$	11.0 mm
$D_{\text{evap},i}$	25.4 mm	$D_{rt,o}$	15 mm
A_t	0.01 m^2	V_{rt}[a]	4.79 cm^3
V_g	42.3 cm^3	$\lambda_{\text{evap}-r}$	0.024 WK^{-1}
$\lambda_{\text{evap}-\infty}$	0.05 WK^{-1}		
Wick		Reservoir	
L_w	199 mm	L_r	62.5 mm
D_{wo}	25.4 mm	D_{ri}	45 mm
D_{wi}	11 mm	A_{ro}	105.5 cm^2
ϵ_w	35%	V_r	98.4 cm^3
D_p	7–12 μm	$\lambda_{r-\infty}$	0.05 WK^{-1}
V_w	82.3 cm^3	H_{bo}	30 $\text{Wm}^{-2}\text{K}^{-1}$

[a]Volume of the bayonet tube is subtracted.

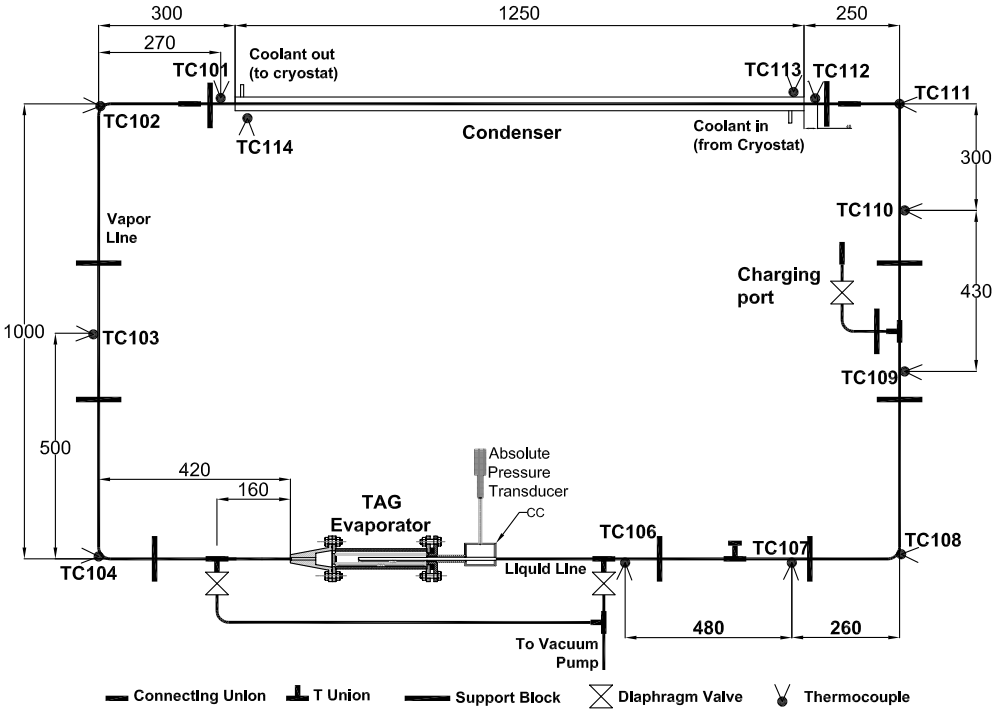

Fig. 4 Schematic of an LHP experimental setup using a TAG evaporator.

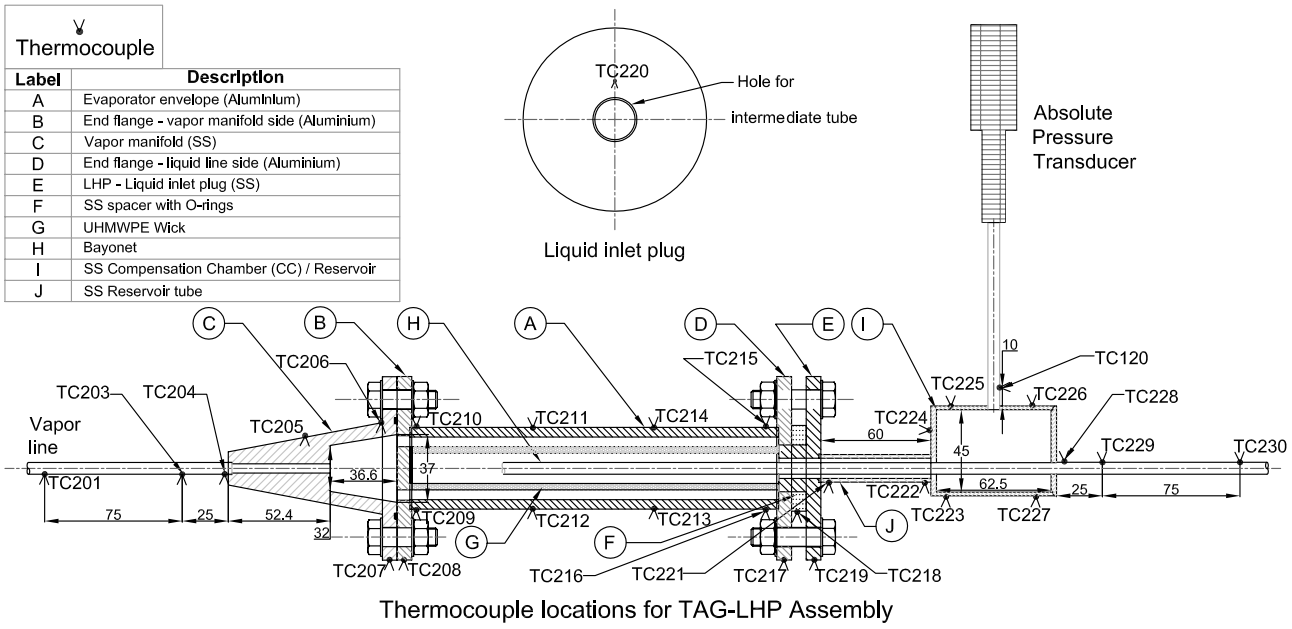

Thermocouple locations for TAG-LHP Assembly

Fig. 5 TAG evaporator assembly for a TAG-LHP.

thermal link. This can be easily achieved by the secondary wick under microgravity conditions for an LHP, which has a structure as shown in Fig. 1. But under terrestrial conditions this may not always be possible. This aspect will be discussed subsequently in this paper.

The LHP is instrumented with several T-type thermocouples for temperature monitoring at various locations shown in Figs. 4 and 5. Two thermocouples TC_{115} and TC_{117} are provided to measure the coolant temperature. These thermocouples are in contact with the fluid, circulated by the cyrostat on the condenser shell side, at the shell inlet and shell exit of the condenser, respectively [15]. The uncertainty in the measurement of all the preceding thermocouples is ± 0.2 K. An absolute pressure transducer (APT) is connected to the reservoir (or the CC). Uncertainty in the measurement of pressure is about 0.5% of full scale. Tape heaters, fixed on the evaporator, are powered by regulated DC power supplies, and the uncertainty in power calculation is less than 1%. The transport lines (liquid and vapor), condenser shell, and the evaporator are insulated with cera-wool and polystyrene. In spite of the insulation, the evaporator loses some heat to the ambient, which is experimentally determined [15]. This has been taken into account during validation.

The loop is charged with 189 g of the R134a. Heat is applied to the evaporator after the cryostat is switched on and the desired condenser temperature reached. All the measurements are displayed in real time and recorded through a computerized data-acquisition system. Each thermocouple is sampled approximately once in 30 s. The steady-state criterion in these experiments for a given load is that all temperature sensors on the evaporator indicate a change of less than 0.1°C in 1 h.

IV. Results and Discussion

The LHP is charged with 189 g of the R134a and is tested with a sink maintained at about −10°C. The test starts with 50 W heat load on the evaporator followed by 25 W increments up to a maximum of 150 W. It takes approximately three hours, on an average, to reach a steady state for each heat load. Heat loads above 150 W are not applied as the evaporator temperature would have exceeded 85°C, which is the maximum allowable temperature for this UHMWPE wick.

A. Experiment

The evaporator and the vapor line temperatures increase with heat load (Fig. 6). The vapor leaving the evaporator is always superheated. As the vapor flows down the vapor line, it loses heat to the ambient. TC_{101} temperatures are lower than T_{sat}, as this location is influenced by conduction heat transfer to the condenser through the tube wall. It may be noted that the evaporator casing temperature is high, indicating that the evaporation heat transfer coefficient is small (about 400 $Wm^{-2}K^{-1}$). The large difference in the evaporator casing temperature and the CC temperature results in larger heat leaks to the CC from the evaporator (Q_{evap-r}). Figure 7 shows the liquid line temperature variation. The temperature at any given location, on the liquid line, reduces as the heat load on the evaporator increases. It is also observed that there is a significant temperature oscillation at almost all locations on the liquid line (Fig. 7). These are attributed to temperature oscillations in the coolant.

Figure 8 shows that the temperature in various parts of the reservoir (CC). The operating temperature can be approximated by the saturation temperature of the fluid in the CC. The saturation temperature in the CC (T_{sat}), shown in Figs. 6 and 8, corresponds to the pressure measured in the CC. The operating temperature does not exhibit the typical $\surd$-shaped curve. The temperature of the CC shows a monotonic rise, unlike that exhibited by an LHP. Although the subcooling available at the exit of the liquid line increases with heat load, the temperature of the CC does not reduce. On further examination of the LHP evaporator construction it is found that though there exists a good hydraulic coupling between the CC and the core, the corresponding thermal coupling depends on the volume of charge in the loop. If the volume of the charge (i.e., the height of liquid in the reservoir) is such that vapor can exist in the reservoir tube and the core, then the reservoir will have a good thermal and hydraulic coupling with the core (Fig. 2b). Under this condition the LHP evaporator would exhibit the $\surd$-shaped operating characteristic. Good thermal coupling allows the subcooled liquid from the bayonet to cool the reservoir as well as the core.

However, when the level of liquid in the reservoir is such that vapor does not exist in the reservoir tube and the core (and the secondary wick is absent), a good hydraulic link and a weak thermal link exist (Fig. 2a). The cause for weak thermal link is that the vapor generated in the reservoir, on account of increased heat leak, cannot travel to the colder core as buoyancy forces limit the downward vapor movement into the core of the evaporator and simultaneous migration of the liquid to the reservoir. This exchange is possible when the level of liquid in the reservoir is lower (i.e., vapor exists in the reservoir tube and the core), allowing such fluid movement. Under such a condition, when the level of liquid is high, the temperature of the reservoir is higher than that of the core, which is subcooled. The CC temperature is determined by the heat balance in

the CC [Eq. (4)]. If the thermal coupling between the liquid in the bayonet and the CC is sufficiently large (or $Q_{\text{evap}-r}$ is very small) to offset for the absence of thermal coupling between the CC and the core. In the present experiment the thermal coupling between the liquid in the bayonet and the CC is small owing to low thermal conductivity of the R134a. Also, a large conduction heat leak to the CC from the evaporator (in comparison to the cooling through bayonet) is present.

It is hypothesized (for terrestrial conditions and a high level of liquid in the reservoir) that in the event of the core being warmer than reservoir (i.e., vapor generation occurs in the core), a good thermal link between the core and the reservoir can be achieved only if a secondary wick is present. The secondary wick aids the flow of liquid from the reservoir to the core and to the primary wick, which results in the vapor shift into the reservoir, thereby rendering a good thermal link between the reservoir and the core. In the absence of a secondary wick, such a fluid exchange cannot be ensured, unless the vapor movement to the CC is assisted by gravity (i.e., buoyancy).

Figure 9 shows the condition ($\beta_{\text{lhp}\to\text{cpl}}$) when the level of liquid is just above the reservoir tube for this reservoir (CC); the volume fraction of liquid in the reservoir under such conditions ($\beta_{\text{lhp}\to\text{cpl}}$) is 0.387. When $\beta < \beta_{\text{lhp}\to\text{cpl}}$, vapor will exist in the core, as a result of which the temperatures of the core and the CC are the same (Fig. 2b). If $\beta > \beta_{\text{lhp}\to\text{cpl}}$ (Fig. 2a), a good thermal link between the CC and the reservoir does not exist. In this experiment, the level of liquid, under all operating conditions, is above the reservoir tube. Calculations indicate β to be about 0.45 in this evaporator. This parameter (β) is based on certain inputs like mass of charge, wick porosity, and length of condensation. If the uncertainty of the volume of liquid in the porous wick is about 5%, the condenser is assumed to be full of liquid, and uncertainty of the mass of the charge (1 g) are all considered, then the calculated volume fraction of the liquid in the reservoir (β) will be more than 0.43. Thus, it can be stated with confidence that in this experiment $\beta > \beta_{\text{lhp}\to\text{cpl}}$. The preceding arguments thus explain the monotonic rise of LHP saturation temperature with heat load.

Higher saturation temperature, as compared with the reservoir tube temperature, indicates that an additional mode of heat transfer (apart from conduction) between the CC and the liquid inlet plug exists. The temperature of the liquid inlet plug (TC_{220} in Fig. 6) is

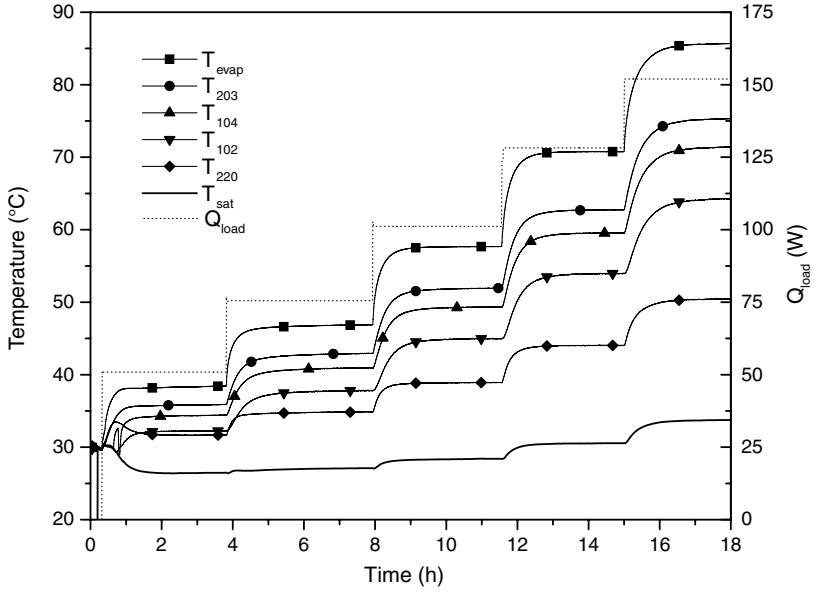

Fig. 6 Transient temperatures of the evaporator and vapor line in the R134a LHP with a TAG evaporator.

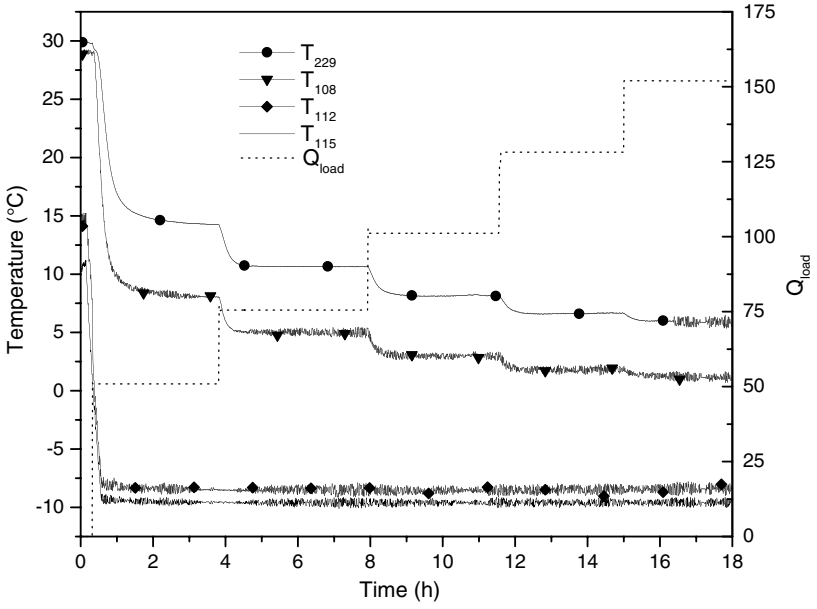

Fig. 7 Transient liquid line temperatures in the R134a LHP with a TAG evaporator.

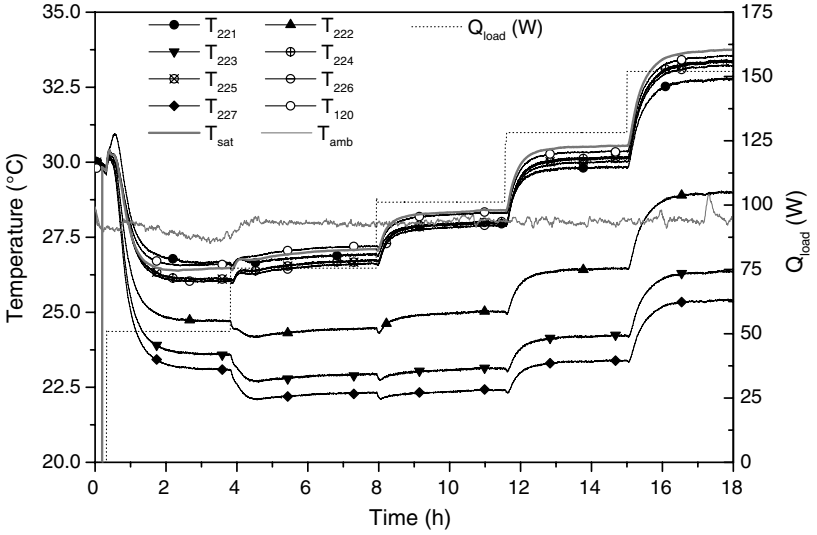

Fig. 8 Transient temperatures of the reservoir and the reservoir tube in the R134a LHP with a TAG evaporator.

significantly larger than the saturation temperature of the fluid in the CC. It is construed so that the vapor generated in the liquid inlet plug migrates to the CC due to buoyancy, as it drifts along the liquid inlet plug.

It is also interesting to observe in Fig. 8 that the temperatures of the reservoir tube as recorded by TC_{221} and TC_{222} are lower than the saturation temperature. With increasing heat loads the temperature difference between them increases. The other temperature sensors at the bottom of the reservoir (TC_{223} and TC_{227}) are also much lower than the saturation temperature of the fluid in the reservoir, with TC_{227} being the coolest. These thermocouples indicate subcooled liquid at the bottom of the reservoir and in the reservoir tube as they are located in the vicinity of the liquid (in the reservoir and reservoir tube) cooled by the bayonet. This suggests that the fluid in the core is a subcooled liquid. Although heat transfer from the evaporator and the ambient to the reservoir (and reservoir tube) is small, it is still significant in determining saturation temperature. The cooler liquid in the bayonet (which passes through the reservoir and the reservoir tube) cools the working fluid around the bayonet to a subcooled state, thus resulting in lower temperatures. The fluid in the CC is thermally stratified. Other temperature sensors on the reservoir follow the saturation temperature (T_{sat} determined from absolute pressure) very closely. Figure 8 shows that TC_{120}, which is on the tube for mounting the APT (Fig. 5), is the closest to T_{sat}, possibly due to film condensation occurring in this tube.

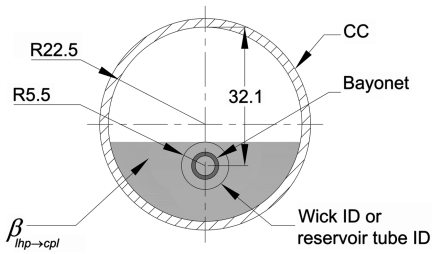

Fig. 9 The minimum liquid inventory in the CC ($\beta_{lhp\rightarrow cpl}$), which can cause a weak thermal link between the CC and the core.

B. Correlation of Predicted Temperatures and Experimental Observation in an R134a Loop Heat Pipe

The operating characteristics do not resemble the typical LHP $\surd$ shape. Its characteristics resemble a CPL, where the reservoir temperature is not externally controlled. The heat leak from the evaporator to reservoir assembly (comprising the liquid inlet plug, reservoir tube, and CC), leak from CC to surroundings and the

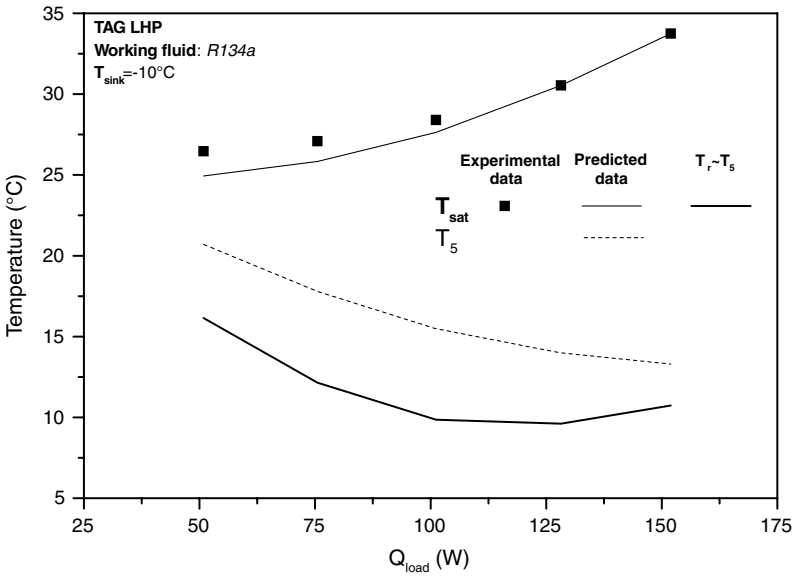

Fig. 10 Effect of core-CC thermal link on the computed LHP operating temperature and their comparison with experimental data.

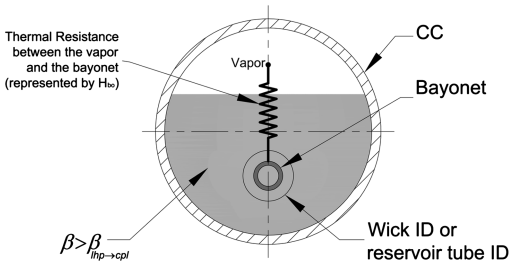

Fig. 11 The bayonet is thermally coupled to vapor in the CC through the liquid surrounding it.

bayonet, determine the temperature (and pressure) in the reservoir. The TAG-LHP is modeled assuming that the fluid in the reservoir is not in thermal communication with that in the core. Algorithm A2-LHP is used where the CC temperature is iteratively determined in conjunction with A1-CPL [5]. The input values required in predicting this LHP operation are summarized in Table 1. The evaporation heat transfer coefficient H_{evap} is evaluated based on the experimental data using following equation:

$$H_{\text{evap}} \approx \frac{Q_{\text{load}}}{A_t(T_{\text{evap}} - T_{\text{sat}})} \tag{11}$$

1. Influence of Liquid Inventory in the Compensation Chamber on the Loop Heat Pipe Operating Temperature

If the operating temperature is obtained based on the model presented in [5], where a good thermal link between the core and the CC exists (i.e., $T_r \sim T_5$), then the CC temperature is expected to reduce with an increase in heat load (Fig. 10). The drop in the CC temperature (or in the operating temperature) with an increase in heat load is ascribed to the increase in subcooling at the inlet of the evaporator. The subcooled liquid entering the core cools both the CC and the core equally well, as a very high thermal coupling exists between the CC and the core. However, when liquid inventory in the CC is large ($\beta > \beta_{\text{lhp}\to\text{cpl}}$), which is observed in the present experiments, the operating temperature would monotonically increase. Figure 10 shows that the predicted and observed CC temperatures differ by less than 2°C. The saturation temperature increases due to increased heat leakage to the CC from the evaporator casing with an increase in heat load on the evaporator. The fluid in the CC is cooled by the cooler liquid in the bayonet. The thermal resistance between the CC vapor and the bayonet (conduction and natural/capillary induced convection (Fig. 2a) through the liquid surrounding the bayonet) primarily determines the temperature difference between the saturation temperature and the liquid temperature in the bayonet at a given heat load (Fig. 11). Figure 10 shows that the predicted core temperature is significantly lower than the operating temperature (i.e., the core is subcooled), which is due to weak thermal coupling between the core and the CC.

2. Evaporator, Vapor Line and Liquid Line Temperatures

The predicted and experimentally determined evaporator temperatures shown in Fig. 12 agree within 2°C. The deviation is attributed to a large heat leak to ambient from the evaporator due to a high evaporator temperature. The predicted temperatures on the vapor line (Fig. 13) and those observed in the experiment differ by 2°C. The vapor in the evaporator vapor grooves undergoes superheating using a model [13] that assumes that the Nusselt number associated with the vapor flow in the vapor grooves is constant. Here superheating of the vapor is estimated based on the assumption of the uniform groove temperature and the Nusselt number (25) in the vapor grooves [15]. This high value of Nusselt number was deduced by correlating the experimental data with the observed temperature. The higher Nusselt number is because the flow in the vapor grooves is developing (thermally and hydrodynamically). The deviations in the predicted evaporator exit temperature propagates down the vapor line. The nonuniform heat transfer coefficient along the vapor line also contributes to a deviation in prediction of the temperature drop in each segment, although the predicted total temperature drop along the vapor line agrees well with experimental observations.

Figure 14 shows the predicted and observed temperature distribution along the liquid line. The Nusselt number in the subcooling region of the condenser is 10 because the thermal and hydraulic development lengths in the experiment are comparable to the subcooling lengths [15]. The predicted temperatures agree with the experimental observations within 3°C. The total temperature drop in the liquid line correlates well with the experimental data.

V. Conclusions

The R134a TAG-LHP in this study, under terrestrial conditions, does *not* exhibit the typical √-shaped operating temperature curve; instead the operating temperature monotonically increases with heat load. This is attributed to the weak thermal link between the CC and the core due to a large liquid inventory in the CC and also to a large heat leak to the CC from the evaporator (due to low evaporation heat transfer). The fluid in the CC exchanges heat with the evaporator, the ambient, the core, and the bayonet passing through the CC. The heat balance in the CC determines its temperature and pressure. In essence, this LHP behaves like a CPL, where the heat balance in the

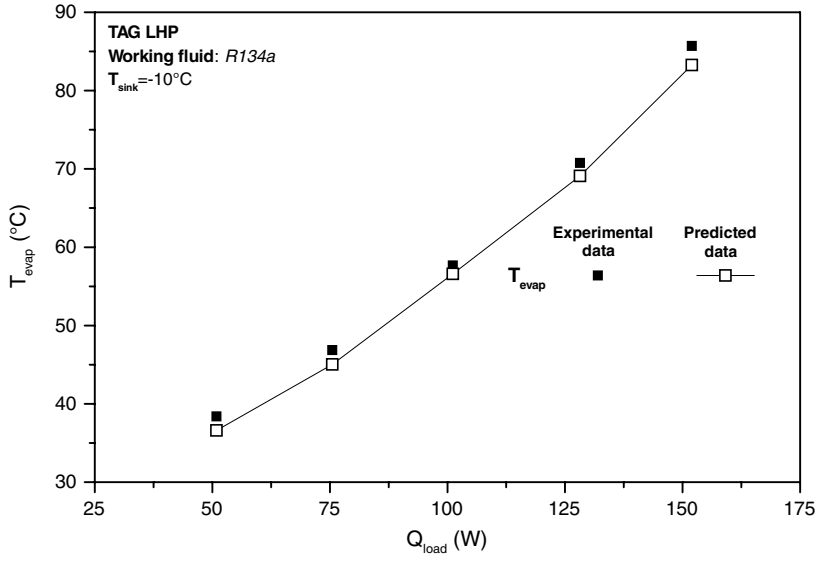

Fig. 12 Predicted and observed evaporator temperatures in the R134a LHP with a TAG evaporator ($T_{\text{sink}} = -10°\text{C}$).

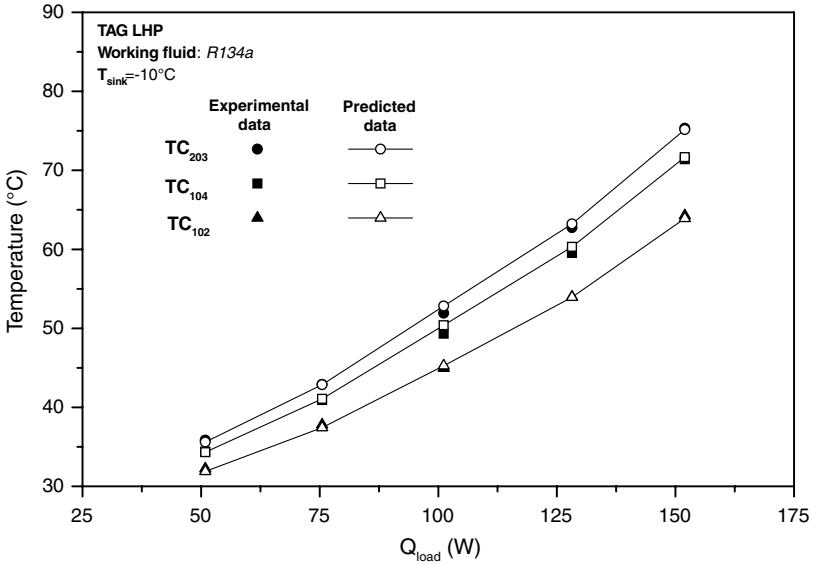

Fig. 13 Predicted and observed vapor line temperatures (TC_{204} to TC_{201}) in the R134a LHP with a TAG evaporator ($T_{sink} = -10°C$).

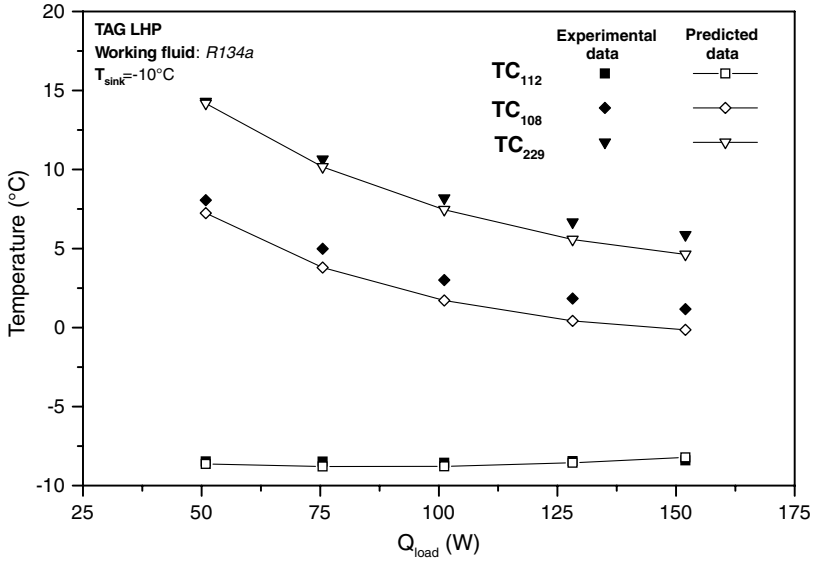

Fig. 14 Predicted and observed liquid line temperatures in the R134a LHP with a TAG evaporator ($T_{sink} = -10°C$).

reservoir determines its temperature and pressure. A mathematical model incorporating this effect was developed and correlated well with experimental data.

The maximum heat load that this LHP transported is 150 W with a mean evaporator temperature of 86°C. The vapor leaving the evaporator is superheated. The liquid line temperatures decrease with an increase in heat load. The predicted and observed CC fluid saturation temperature agree within 2°C. The correlation exercise indicates that the predicted and observed temperatures in the evaporator, the vapor line, and the liquid line temperatures differ by less than 4°C.

The present study clearly demonstrates that LHPs, which have been conventionally used for space application, can be used in terrestrial applications. For such applications, the mass of charge is to be determined by also taking into account the thermal link between the CC and the core. The impact of liquid inventory on the CC core thermal link could also be investigated in LHPs with multiple evaporators or with dual CCs.

Acknowledgments

This work was carried out at ISRO Satellite Center. The authors are grateful to D. R. Bhandari, K. Badari Narayana, S. G. Barve, and D. Chakraborty (from ISRO Satellite Center) for encouragement and support.

References

[1] Ku, J., "Operating Characteristics of Loop Heat Pipes," Society of Automotive Engineers, Paper No. 1999-01-2007, 1999.

[2] Maidanik, Y. F., "Loop Heat Pipes," *Applied Thermal Engineering*, Vol. 25, April 2005, pp. 635–657. doi:10.1016/j.applthermaleng.2004.07.010

[3] Ku, J., "Thermodynamic Aspects of Capillary Pumped Loop Operation," *6th AIAA/ASME Joint Thermophysics and Heat Transfer Conference*, AIAA Paper 94-2059, 1994.

[4] Ku, J., "Recent Advances in Capillary Pumped Loop Technology," *National Heat Transfer Conference*, AIAA Paper 97-3780, 1997.

[5] Adoni, A. A., Ambirajan, A., Jasvanth, V. S., Kumar, D., Dutta, P., and Srinivasan, K., "Thermohydraulic Modeling of Capillary Pumped Loop and Loop Heat Pipe," *Journal of Thermophysics and Heat Transfer*, Vol. 21, No. 2, 2007, pp. 410–421. doi:10.2514/1.26222

[6] Launay, S., Sartre, V., and Bonjour, J., "Parametric Analysis of Loop Heat Pipe Operation: A Literature Review," *International Journal of Thermal Sciences*, Vol. 46, 2007, pp. 621–636. doi:10.1016/j.ijthermalsci.2006.11.007

[7] Pastukhov, V. G., Maidanik, Y. F., and Fershtater, Y. G., "Adaption of

Loop Heat Pipes to Zero-G Conditions," *Proceedings of the Sixth European Symposium on Space Environmental Control Systems*, European Space Agency, ESA SP-400, 1997, pp. 385–391.

[8] Dickey, J. T., and Peterson, G. P., "Experimental and Numerical Investigation of a Capillary Pumped Loop," *Journal of Thermophysics and Heat Transfer*, Vol. 8, No. 3, 1994, pp. 602–607. doi:10.2514/3.584

[9] Kaya, T., and Hoang, T. T., "Mathematical Modelling of Loop Heat Pipes and Experimental Validation," *Journal of Thermophysics and Heat Transfer*, Vol. 13, No. 3, 1999, pp. 314–320. doi:10.2514/2.6461

[10] Guiping, L., Hongxing, Z., Xingguo, S., Jianfeng, C., Ting, D., and Jianyin, M., "Development and Test Results of a Dual Compensation Chamber Loop Heat Pipe," *Journal of Thermophysics and Heat Transfer*, Vol. 20, No. 4, 2006, pp. 825–834. doi:10.2514/1.21858

[11] Launay, S., Sartre, V., and Bonjour, J., "Analytical Model for Characterization of Loop Heat Pipes," *Journal of Thermophysics and Heat Transfer*, Vol. 22, No. 4, 2008, pp. 623–631. doi:10.2514/1.37439

[12] Hoang, T. T., Sukhov, D. A., Baldauff, R. W., and Cheung, K. H., "Issues with LHP Testing in 1-*g* Environment," *Proceedings of the 9th AIAA/ASME Joint Thermophysics and Heat Transfer Conference*, AIAA Paper 2007-4158, 2007.

[13] Adoni, A. A., Ambirajan, A., and Jasvanth, V. S., "Aspects of Thermohydraulic Modelling of Capillary Pumped Loop and Loop Heat Pipe," ISRO Satellite Center, Rept. ISRO-ISAC- TR-0809, Bangalore, India, June 2007.

[14] Chapra, S. C., and Canale, R. P., *Numerical Methods for Engineers*, McGraw–Hill, New York, 2002.

[15] Adoni, A. A., Ambirajan, A., and Jasvanth, V. S., "Analyses of Results from Experiments on Capillary Pumped Loop and Loop Heat Pipe," ISRO Satellite Centre, Rept. ISRO- ISAC-TR-0845, Bangalore, India, March 2008.